



# A decentralized impedance-based adaptive droop method for power loss reduction in a converter-dominated islanded microgrid



Konstantinos O. Oureilidis, Charis S. Demoulias\*

Department of Electrical and Computer Engineering, Aristotle University, Thessaloniki, 54124, Greece

## HIGHLIGHTS

- A new decentralized adaptive droop control method is proposed.
- Reduction of line losses is achieved in comparison to the conventional droop method.
- The droop coefficients are adjusted by the microgrid impedance sensed by each DER.
- The active and reactive power are decoupled by the adaptive droop coefficients.
- The proposed method can be applied irrespective of the microgrid topology.

## ARTICLE INFO

### Article history:

Received 5 May 2015

Received in revised form

14 August 2015

Accepted 4 November 2015

Available online 21 November 2015

### Keywords:

Microgrid

Distributed energy sources

Power losses

Droop control

Adaptive droop coefficients

## ABSTRACT

As the integration of Distributed Energy Resources (DERs) in modern grids is increasing, the microgrid concept has been established. In the case of converter-dominated microgrids without communication links, the droop control method is mainly adopted in the primary control level. Normally, the economic operation of the microgrid is incorporated in the secondary control level, requiring communication among the DERs and a central controller. On the contrary, this paper proposes an adaptive droop control method based on local measurements, which achieves a power sharing with reduced power losses within the islanded microgrid. The droop coefficients are adjusted by calculating the microgrid impedance, sensed by each DER. Therefore, the remote DERs calculate a large impedance and inject lower active and reactive power, reducing the line losses. The location and the size of the DERs and the loads can be arbitrary. Another advantage is the absence of the virtual impedance control, as the power decoupling is implemented inherently by the adaptive droop coefficients. The effectiveness of the proposed control strategy is verified by extended simulation results in comparison with the accurate sharing method for different microgrid topologies.

© 2015 Elsevier Ltd. All rights reserved.

## 1. Introduction

The development of cleaner and more reliable power grids with distributed power sources has created the microgrid concept [1]. As small-scale power sources are connected to the microgrid through DC/AC or AC/DC/AC converters, the proper control of the converters has drawn considerable attention [2]. According to IEEE 1547.4, the microgrid systems should combine the capability of a dual operation, either in grid-connected or island mode. The grid-connected mode aims to inject the available power to the grid, determined by a maximum power point tracking strategy [3]. On the other side, in island mode, the power production

should fulfill the load demand, while the voltage and the frequency are maintained within the permissible limits. This operation mode may modify the injected power to a less efficient operation point.

During island operation, the DERs are in charge for balancing the voltage profile within the microgrid and ensure a proper power sharing [4]. In this primary control level, the conventional droop control method is mainly adopted [5–7] and is implemented without any communication infrastructure. In case of inductive line impedances, the frequency of the microgrid is formed by the total injected active power, while the node voltage by the respective reactive power [8]. This control law should be inverted in case of purely resistive microgrids [9,10]. In fact, in most cases the impedance is complex [10], consequently a proper power sharing is hard to be achieved by the conventional droop control method. For this reason, a virtual impedance control is used in order to modify the voltage input of the droop control and ensure an accurate

\* Corresponding author. Tel.: +30 2310995960.

E-mail address: [chdimoul@auth.gr](mailto:chdimoul@auth.gr) (C.S. Demoulias).

power sharing among the DERs [9,10]. As accurate is defined the power sharing, where each DER supplies active and reactive power in proportion to its nominal apparent power. The value of the virtual impedance is calculated for a given microgrid topology, while it can be updated automatically in case of a topology change by using communication signals [11,12]. On the other hand, when the communication is not available, the proper power sharing cannot be guaranteed.

Concerning the influence of the power sharing on the line losses, it is demonstrated in [13] that the power sharing modification due to the line impedance mismatch can lead to line loss reduction. However, only resistive microgrids are considered. In [14], an on-line Optimization Strategy based on local measurements is adopted, in order to define the optimal reactive power settings of each DER, so as the power losses along the feeder are minimized. The drawback concerns the modeling approximations, since the control can be integrated to only one DER. In [15], the proposed control strategy consists of an adaptive droop controller, in respect with the local reactive power. This methodology is implemented in medium voltage microgrids, where the R/X ratio is low and the losses can be reduced without considering the active power regulation. Nevertheless, this assumption cannot be adopted for low-voltage grids. Other decentralized methodologies based on local measurements focus only on the reactive power dispatch in order to reduce losses [16–18].

Alternatively, an economic operation of the microgrid can be achieved by deploying a microgrid central controller (MGCC) with low-bandwidth communication infrastructure. This control level is characterized as secondary control [7] and is based on evaluating measurements collected by the power production and consumption. In order to obtain the maximum benefits from the DERs operation, the power dispatch reaches to the optimal or near optimal operation point by solving a power flow problem [19] and updating appropriately each droop characteristics [20,21]. In [22,23] a MGCC multi-stage optimization algorithm is implemented to minimize the fuel consumption of a droop-controlled islanded microgrid, without considering the operational constraints of the voltage and the frequency. In [24] the presented multi-stage optimization takes into account the system power losses and the operational constraints. In [25,26] different algorithms propose the economic dispatch of the DERs. A method for grid-connected grids with PVs is presented in [27], where the multi-objective configuration concerns only the reactive power for minimizing the power losses. In order to provide the highest possible autonomy to the DERs, decentralized methodologies based on Multi-Agent Systems (MAS) have also been developed [28–31]. However, the communication is still considered necessary.

Furthermore, various other methods have been proposed for loss minimization by means of distributed generation integration [32,33]. The most important are concentrated on capacitor placement, cooperation with Flexible AC Transmission Systems (FACTS), energy storage allocation, feeder reconfiguration and DG allocation. However, these methodologies use complex mathematical tools, while they assume a known topology for the DG placement. Furthermore, in many cases, the communication is regarded necessary.

This paper proposes a new power sharing methodology for converter-dominated islanded microgrids for achieving reduced line losses in comparison to the conventional droop method. The proposed control strategy adapts the droop coefficients, according to a microgrid impedance sensed by each DER. Therefore, the DERs closer to the loads are forced to supply them in priority, leading to power flows through smaller line impedance routes. The proposed method can be adopted in any arbitrary microgrid topology, while no communication is needed. Furthermore, the implementation of virtual impedance control is no longer necessary, as the

different impedances of the power lines are taken into account indirectly in the adaptive droop coefficients. Since the proposed control strategy relies only on local measurements, the function of loss reduction is implemented in the primary control level, instead of the secondary control level. The proposed method is compared with the accurate power sharing methodology, proving its effectiveness in line loss reduction.

The accurate power sharing with virtual impedance control strategy is explained in Section 2, while Section 3 presents the proposed adaptive droop control strategy. In Section 4, both looped and radial topologies are examined. Finally, Section 5 contains the conclusions.

## 2. Power sharing with conventional droop control

The conventional wireless droop method functions by emulating a traditional power system with parallel synchronous generators. In this method, the microgrid frequency and voltage serve as communication parameters for all DERs. Therefore, the active and reactive power of the loads are shared among the connected DERs without using physical communications among them [5,6]. Considering inductive line impedances, the control law imposes the determination of the microgrid frequency  $f$  from the active power  $P$ , while the node voltage  $V_n$  is determined by the reactive power  $Q$ ,

$$f = f_0 - m \cdot P - m_d \frac{dP}{dt} \quad (1)$$

$$V_n = V_0 - n \cdot Q - n_d \frac{dQ}{dt} \quad (2)$$

where  $f_0$ ,  $V_0$  correspond to the frequency and voltage magnitude at no-load operation,  $m$ ,  $n$  are the droop control coefficients and  $m_d$ ,  $n_d$  are the derivative droop coefficients.

The active and reactive power are calculated by transforming in the rotating  $dq$  frame the voltage and the current at the LC output filter of each DER:

$$P = \frac{3}{2} (V_d I_d + V_q I_q) \quad (3)$$

$$Q = \frac{3}{2} (V_d I_q - V_q I_d) \quad (4)$$

where  $V_d$ ,  $I_d$  are the direct axis components of the voltage and the current and  $V_q$ ,  $I_q$  are the respective quantities in the quadrature axis.

The slope parameters of the conventional droop control  $m$  and  $n$  are set proportional to the maximum power of the DER [5–13], in respect to the permissible frequency and voltage variation. The purpose is to achieve a power sharing in proportion to the nominal power of each DER.

However, the line impedance in low-voltage microgrids rarely is purely inductive. In most cases consists of both resistive and inductive part [10]. With complex impedances, an efficient power sharing cannot be achieved, due to the coupled active and reactive power characteristic of the system. As a result, reactive currents are circulating among the DERs, increasing significantly the power losses on the connection lines. In order to overcome this problem, the output voltage is adjusted according to the virtual impedance control [5–12]. The advantages of using a virtual instead of a physical impedance is attributed to the increased cost, weight and power losses.

Additionally, the virtual impedance control aims at sharing the power accurately among the connected DER. For this reason, the value of the virtual impedance is adjusted differently for each DER, taking into consideration the relative distance of each DER to the common ac bus of the microgrid. This value is usually

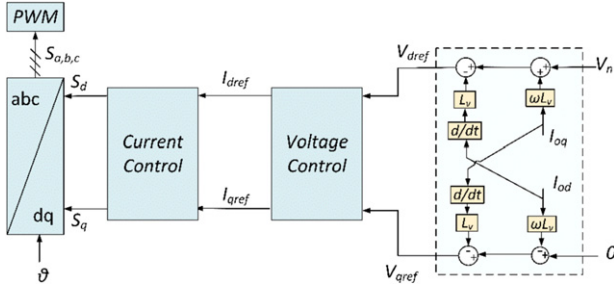


Fig. 1. Droop control with inductive virtual impedance.

larger than the physical line impedances. In order to enhance the effectiveness of the virtual impedance, a communication infrastructure is considered necessary.

Fig. 1 presents the conventional droop control with an inductive virtual impedance. By selecting a large virtual induction ( $L_v$ ), the inductive behavior of the droop control law is also ensured [8]. The currents  $I_{od}$  and  $I_{oq}$  are the output currents of each DER. The content of the voltage and current control are analyzed in a following figure.

### 3. Proposed adaptive droop control methodology

According to the previous section, the virtual impedance cannot be regarded as a global parameter, but it depends on the distance of each DER from the common ac bus. The situation is even more complicated in case of looped or meshed microgrids, where the common ac bus is absent. Furthermore, a static calculation of the virtual impedance provokes problems when extending an existing microgrid by adding new DERs. In such a case, new virtual impedance calculations are necessary, which implies new settings for all the DERs.

Another important issue concerns the power losses. An accurate power sharing cannot guarantee an optimal power distribution. Considering the virtual impedance setting, the distance from the DERs to the loads should also be taken into account. However, the load profiles usually include many fluctuations, which raises concerns about the proper adjustment of the magnitude of the virtual impedance.

In this paper, a new power sharing methodology is developed. The power sharing is performed through the droop control law, with adaptive droop coefficients. The droop coefficients are adjusted in accordance with the microgrid impedance sensed by the ac terminals of each DER. Since the distance to the loads is not the same, the microgrid impedance is different for each DER. The proposed control strategy can be used regardless of the microgrid topology (radial, looped or meshed). As the droop coefficients depend on the microgrid impedance, the electrical parameter of the connection lines are taken into consideration. Therefore, the coupling among the active and reactive power is achieved, which makes the virtual impedance unnecessary.

#### 3.1. Microgrid impedance calculation

Firstly, the microgrid impedance, as sensed by each DER, should be calculated. Since no communication is available, a distortion signal is added to the output current of each DER, while its feedback is measured in the voltage at the respective point of connection with the microgrid by implementing a Phase-Locked Loop (PLL). The proposed distortion signal is inserted in the control strategy by intentionally disturbing the control angle  $\theta$  of the conventional droop control of each DER by a parameter proportional to the sinusoid of the angle. This particular distortion is selected, because it does not affect the

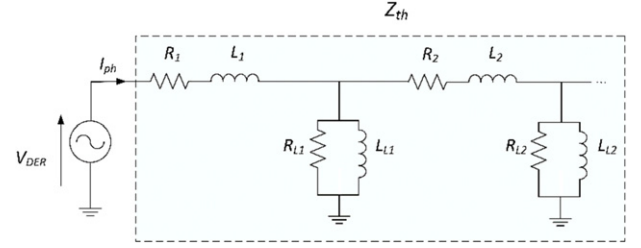


Fig. 2. Equivalent Thevenin impedance at the terminals of one DER.

zero-crossing of the voltage [34]. The initial angle is calculated by the frequency of the  $P$ - $f$  droop curve:

$$\theta = \int 2\pi f dt. \quad (5)$$

The new control angle  $\theta_c$  contains the disturbance signal  $\sin \theta$  and can be described by the following equation:

$$\theta_c = \theta + k \sin \theta. \quad (6)$$

The value of  $k$  is selected so as not to exceed the harmonic limitations of the voltage. For this reason, it takes a quite small value. Considering the angle distortion, the phase current  $I_{ph}$  of a DER can be expressed as:

$$I_{ph} = \sqrt{2} \cdot I_{rms} \sin(\theta + k \sin \theta). \quad (7)$$

Since  $k \sin \theta$  is very small,  $\cos(k \sin \theta) \approx 1$  and  $\sin(k \sin \theta) \approx k \sin \theta$ . Thus, (7) is transformed to:

$$I_{ph} = \sqrt{2} I_{rms} \left( \sin \theta + \frac{k}{2} \sin 2\theta \right). \quad (8)$$

The current is analyzed into two components; the first is the same to the conventional droop control, while the second assigns to the disturbance. The disturbance creates a kind of second harmonic voltage equal to  $\frac{k}{2} \sqrt{2} I_{rms} Z_{th}$ , where  $Z_{th}$  is a sort of Thevenin impedance sensed by the terminal of each DER. The impedance takes into account all the line and load impedances within the microgrid, as shown schematically in Fig. 2. According to EN 50160 Standard [35] for weak islanded grids, the magnitude of the second harmonic voltage should not exceed 2% of the respective voltage magnitude in the fundamental frequency ( $\sqrt{2} I_{rms} Z_{th}$ ). Therefore, the gain  $k$  should be smaller than 0.04.

The feedback of the disturbance can be calculated through the Park Transformation of the phase voltages of each DER by implementing a  $d$ - $q$  PLL, as it is presented in the control strategy of the converter in Fig. 3.

$$\begin{bmatrix} V_{mgd} \\ V_{mgq} \\ V_{mg0} \end{bmatrix} = \sqrt{\frac{2}{3}} \begin{bmatrix} \cos \theta_{PLL} \cos \left( \theta_{PLL} - \frac{2\pi}{3} \right) \cos \left( \theta_{PLL} + \frac{2\pi}{3} \right) \\ \sin \theta_{PLL} \sin \left( \theta_{PLL} - \frac{2\pi}{3} \right) \sin \left( \theta_{PLL} + \frac{2\pi}{3} \right) \\ \frac{\sqrt{2}}{2} \quad \frac{\sqrt{2}}{2} \quad \frac{\sqrt{2}}{2} \end{bmatrix} \cdot \begin{bmatrix} V_a \\ V_b \\ V_c \end{bmatrix} \quad (9)$$

$$\begin{bmatrix} V_a \\ V_b \\ V_c \end{bmatrix} = \begin{bmatrix} \sqrt{2} V_{rms} \sin \theta_c \\ \sqrt{2} V_{rms} \sin \left( \theta_c - \frac{2\pi}{3} \right) \\ \sqrt{2} V_{rms} \sin \left( \theta_c + \frac{2\pi}{3} \right) \end{bmatrix}. \quad (10)$$



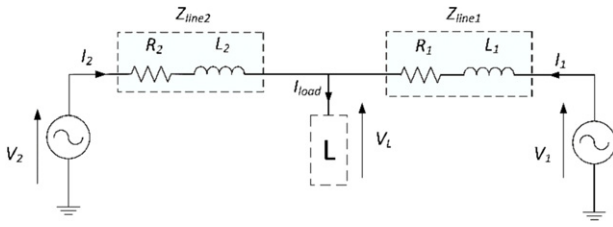


Fig. 4. Radial microgrid with 2 DERs.

proposed control strategy can be overridden, so as the droop coefficients are directly set by the MGCC. In this case, the power output of each DER is determined by the secondary control strategy. This overriding option is shown in Fig. 3 with the MGCC and Secondary Control boxes. However, since this paper is concentrated only on implementing control strategies based on local measurements, the secondary control is not analyzed.

A remote DER senses a relatively larger  $Z_{th}$  compared to a DER closer to the loads, therefore the respective droop coefficients take larger values. As the frequency is a global parameter, the injected active power of the remote DER is reduced compared to the conventional droop methodology. To demonstrate the implementation of the proposed strategy, the simple case of two DERs of the same apparent power feeding a common load with different connection lines (Fig. 4) is used. Initially, both DERs have the same droop settings ( $m_1 = m_2, n_1 = n_2$ ) and inject the same active and reactive power, as shown in Fig. 5. In this stage, the power losses in per phase base are calculated by:

$$P_{loss} = I_1^2 \cdot R_1 + I_2^2 \cdot R_2. \quad (18)$$

Under accurate power sharing, the two currents have approximately the same magnitude ( $I_1 \approx I_2$ ), regardless of the difference in the line resistances. However, in the case under study,  $R_2$  is considered  $\lambda$  times the resistance  $R_1$ , where  $\lambda > 1$ . The total power losses are described by:

$$P_{loss} = I_2^2 \cdot R_1 \cdot (1 + \lambda). \quad (19)$$

The load current  $I_{load}$  equals the aggregation of the DERs currents, which can be expressed by  $I_2$  as:

$$I_{load} = 2 \cdot I_2. \quad (20)$$

By implementing the proposed adaptive droop control, the droop curves are adjusted according to Fig. 5. As the currents become proportional to the impedance, the voltage drop from each DER to the load becomes also the same. For this reason, the voltage  $V_n$  (described in (2)) becomes a global parameter. Due to the absence of the virtual impedance control, the direct voltage component  $V_d$  is equal to  $V_n$ , while the respective quadrature component  $V_q$  is equal to zero. The injected current can be analyzed in the respective active and reactive component:

$$I'_i = I'_{d,i} + jI'_{q,i} \quad (21)$$

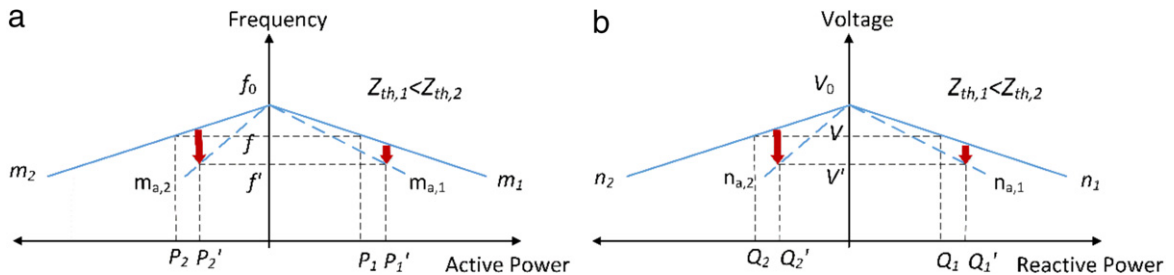


Fig. 5. (a) P-f droop control, (b) Q-V droop control.

$$I'_{d,i} = \frac{2P'}{3V'_d} \quad (22)$$

$$I'_{q,i} = \frac{2Q'}{3V'_d} \quad (23)$$

for  $i = 1, 2$ .

The new values of the active and reactive power can be obtained by the droop control, considering the proposed adaptive droop coefficients. The derivative terms of droop control can be omitted, as their contribution is restricted to transients. Therefore, each current is formed as:

$$I'_i = \frac{2}{3} \frac{f_0 - f'}{m_{a,i} \cdot V'_d} + j \frac{2}{3} \frac{V_0 - V'_d}{n_{a,i} \cdot V'_d} \quad (24)$$

where  $f'$  and  $V'_d$  are the new operating frequency and voltage.

According to (15) and (16),  $m_{a,2} = \lambda \cdot m_{a,1}$  and  $n_{a,2} = \lambda \cdot n_{a,1}$ , as  $Z_{th2} = \lambda \cdot Z_{th1}$ . By replacing the droop coefficients in (24), the current of DER<sub>1</sub> becomes  $\lambda$  times the current of DER<sub>2</sub>. The load current is now expressed by:

$$I_{load} = I'_1 + I'_2 = \lambda \cdot I'_2 + I'_2 = I'_2 \cdot (\lambda + 1). \quad (25)$$

Considering that the load current remains the same, (20) and (25) are equal, thus:

$$I_2 = \frac{I'_2 \cdot (\lambda + 1)}{2}. \quad (26)$$

The power losses after the implementation of the proposed adaptive droop are calculated as:

$$P'_{loss} = I_1'^2 \cdot R_1 + I_2'^2 \cdot R_2 = I_2'^2 \cdot R_1 \cdot \lambda \cdot (1 + \lambda). \quad (27)$$

By dividing the power losses under the accurate power sharing with the respective losses under the proposed control:

$$\frac{P_{loss}}{P'_{loss}} = \frac{I_2^2 \cdot R_1 \cdot (1 + \lambda)}{I_2'^2 \cdot R_1 \cdot \lambda \cdot (1 + \lambda)} = \frac{(1 + \lambda)^2}{4\lambda} > 1. \quad (28)$$

The last term is always larger than 1, as  $(1 + \lambda)^2 > 4\lambda \Rightarrow (1 - \lambda)^2 > 0$ . As a result, the power losses are always reduced. The analysis of the simple two DER case can be generalized for a microgrid with many sources and loads.

#### 4. Simulation tests

In order to demonstrate the effectiveness of the proposed droop control methodology with adaptive droop coefficients, several simulation tests are conducted with PSIM software. The low-voltage microgrid operates at 400 V line voltage, while the loads are simulated as constant-power balanced three-phase loads. The DC voltage of each primary source is 800 V and the switching frequency of the converters is 9.95 kHz. The following cases are investigated for looped and radial microgrid topologies.

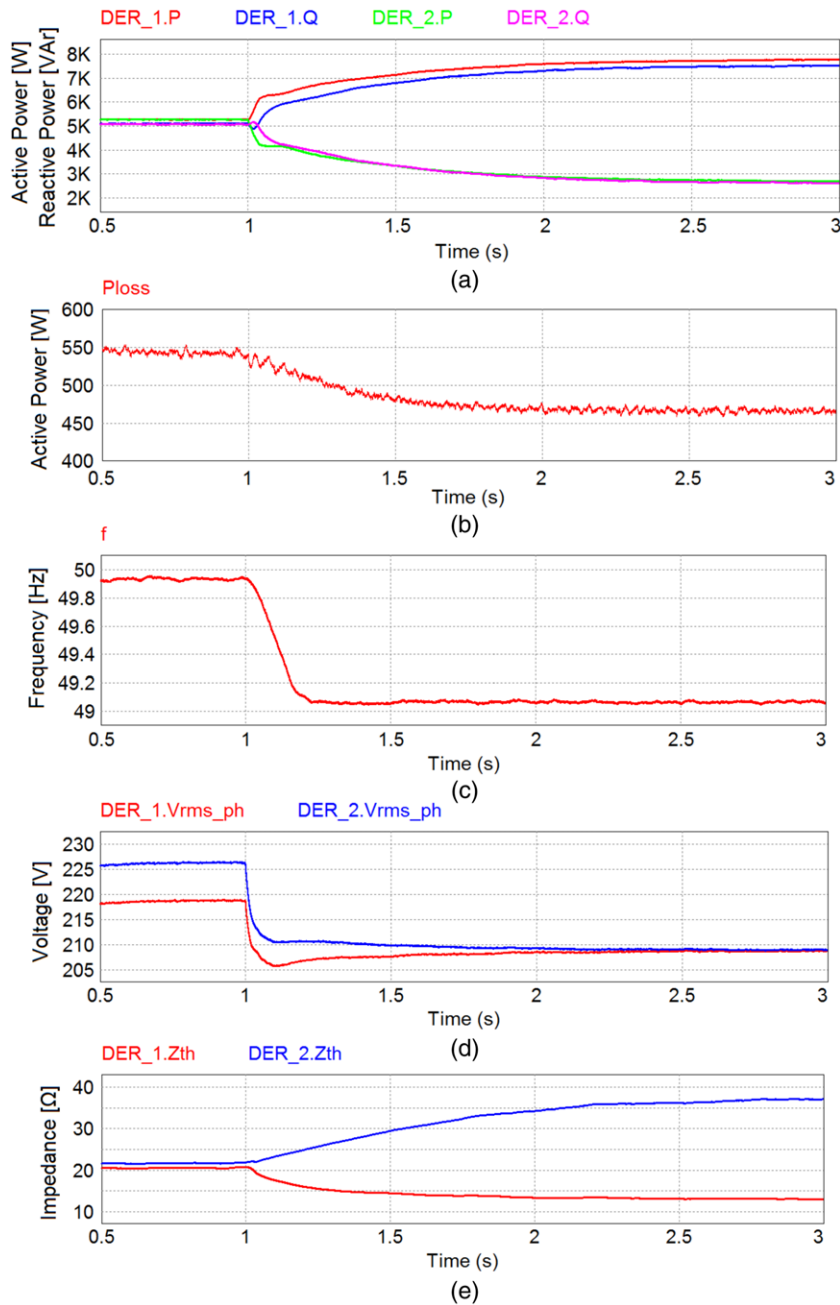


**Fig. 6.** Simulation results of a microgrid with two DERs: (a) active (W) and reactive (VAr) power, (b) power losses (W), (c) frequency (Hz), (d) rms phase voltage magnitude (V), (e) microgrid impedance ( $\Omega$ ).

#### 4.1. Two DERs of the same power in radial topology

In the first simulation test, the previous example of two DERs (Fig. 4) is analyzed. The DERs have the same active power of 10 kW, feeding a load of 10 kW and 10 kVAr. The connection lines are of ACSR 16 mm<sup>2</sup> type with  $R = 1.268 \Omega/\text{km}$  and  $L = 1.3432 \text{ mH}$ , while the length of the connection lines are  $\text{Line}_1 = 300 \text{ m}$  and  $\text{Line}_2 = 900 \text{ m}$ . At the beginning, the DERs operate according to the conventional droop control adjusted with the virtual impedance. The initial settings of the droop coefficients are  $m_1 = m_2 = 2 \cdot 10^{-4}$  and  $n_1 = n_2 = 3.25 \cdot 10^{-3}$ . In order to achieve an accurate power sharing, the values of the virtual impedances must be 0.2 mH for DER<sub>1</sub> and 3.47 mH for DER<sub>2</sub>. At  $t = 1$  s, the proposed control methodology adjusts the droop coefficients according to the calculated microgrid impedance. The active and reactive power of DER<sub>1</sub> are increased, while the respective power of DER<sub>2</sub> is decreased

(Fig. 6(a)). The total power losses before and after the proposed control are presented in Fig. 6(b), where the reduction from 543.5 to 466.4 W (14.19%) in comparison with the accurate power sharing can be verified. In the new operation point, the frequency of the microgrid is decreased (Fig. 6(c)), while the node voltages become equal (Fig. 6(d)). According to Fig. 6(e), the calculated impedance of DER<sub>2</sub> changes to three times the respective impedance of DER<sub>1</sub>, following the ratio of the corresponding line impedances.

#### 4.2. Microgrid with 4 DERs in looped topology

The next simulation test concerns a microgrid with four DERs and three three-phase loads, as it is illustrated in Fig. 7. The parameters of the DERs and loads are presented in Tables 1 and 2 respectively. The connection lines are ACSR 16 mm<sup>2</sup>, while the distances are  $\text{Line}_1 = 300 \text{ m}$ ,  $\text{Line}_2 = 1500 \text{ m}$ ,  $\text{Line}_3 = 200 \text{ m}$ ,

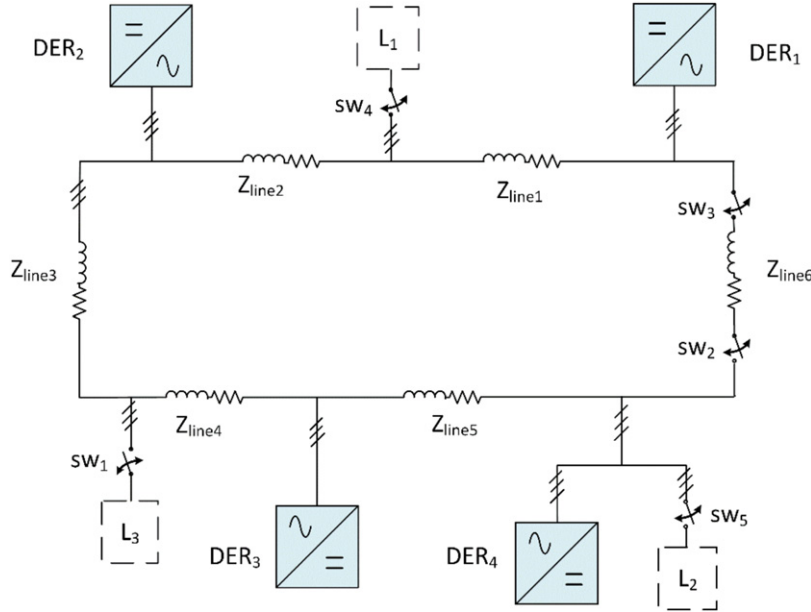


Fig. 7. Microgrid simulation model.

Table 1  
DER parameters.

	DER <sub>1</sub>	DER <sub>2</sub>	DER <sub>3</sub>	DER <sub>4</sub>
Rated power $P$ (kW)	10	3	12	15
Nominal apparent power $S_{nom}$ (kVA)	12.5	3.75	15	18.75
Filter inductance $L_f$ (mH)	2	0.6	2.4	3
Filter capacitance $C_f$ ( $\mu$ F)	15	50	12.5	10
Nominal frequency droop coefficient $m$	$2 \cdot 10^{-4}$	$6.67 \cdot 10^{-4}$	$1.66 \cdot 10^{-4}$	$1.33 \cdot 10^{-4}$
Nominal amplitude droop coefficient $n$	$3.25 \cdot 10^{-3}$	$10.83 \cdot 10^{-3}$	$2.7 \cdot 10^{-3}$	$2.16 \cdot 10^{-3}$
Derivative coefficients $m_d, n_d$	$10^{-5}$	$10^{-5}$	$10^{-5}$	$10^{-5}$
Nominal impedance $Z_{nom}$ ( $\Omega$ )	12.8	42.67	10.67	8.53

Table 2  
Load active and reactive power.

	L <sub>1</sub>	L <sub>2</sub>	L <sub>3</sub>
Active power $P$ (kW)	13	17.5	4
Reactive power $Q$ (kVar)	6.5	8	2

Line<sub>4</sub> = 100 m, Line<sub>5</sub> = 600 m, Line<sub>6</sub> = 150 m. Table 3 presents the required virtual impedance settings in order to achieve accurate power sharing. The switches sw<sub>2</sub> and sw<sub>3</sub> are used to transform the microgrid topology from looped to radial, while switches sw<sub>1</sub>, sw<sub>4</sub> and sw<sub>5</sub> are used for connecting/disconnecting the respective loads. At the beginning, the microgrid operates according to the conventional droop control, where each DER supplies the total microgrid load in proportion to its nominal power.

#### 4.2.1. Case study 1: looped microgrid with L<sub>1</sub> and L<sub>2</sub> connected

At  $t = 1$  s, as shown in Fig. 8, the proposed control is implemented and the droop coefficients are adjusted according to the measured microgrid impedance. The  $Z_{th}/Z_{nom}$  ratio of each DER is

presented in Fig. 8(f). Accounting that L<sub>2</sub> shares a common bus with DER<sub>4</sub>, the latter tries to cover this load, reaching its maximum available power (Fig. 8(a), (b)). The remaining power demand of L<sub>2</sub> ( $17.5 - 15 = 2.5$  kW) and the total power demand of L<sub>1</sub> should be fulfilled by the remaining three DERs. Since DER<sub>1</sub> and DER<sub>2</sub> are relatively closer to these loads, they also reach their maximum power, while DER<sub>3</sub> supplies with the difference (as being the most distant). Therefore, the new power balance is achieved by operating the DERs away from their accurate-power-sharing operating point. The loads are fulfilled with a lower frequency (Fig. 8(d)), while the node voltages at each DER are also lower and equal. The power losses are reduced from 914.8 to 597 W, corresponding to 34.74% loss reduction.

#### 4.2.2. Case study 2: looped microgrid with connection of L<sub>3</sub>

At  $t = 3$  s, L<sub>3</sub> is connected to the microgrid. After a small transient, the microgrid settles at a slightly different operation point of frequency and voltage (Fig. 8(d), (e)). At this operation point, the power losses are still reduced, compared to the conventional droop strategy (from 751.9 W with accurate power

Table 3  
Virtual impedance settings.

Microgrid topology	DER <sub>1</sub> (mH)	DER <sub>2</sub> (mH)	DER <sub>3</sub> (mH)	DER <sub>4</sub> (mH)
Looped topology with L <sub>1</sub> , L <sub>2</sub>	0.75	11.38	4.52	0.21
Lopped topology with L <sub>1</sub> , L <sub>2</sub> , L <sub>3</sub>	0.02	40.55	3.23	0.384
Looped topology with L <sub>2</sub> , L <sub>3</sub>	3.38	41.24	5.46	1.36
Radial topology with L <sub>1</sub> , L <sub>2</sub>	3.35	4.89	0.48	11.13
Radial topology with L <sub>1</sub> , L <sub>2</sub> , L <sub>3</sub>	3.36	11.28	3.24	0.14
Radial topology with L <sub>1</sub> , L <sub>3</sub>	9.89	46.27	4.02	18.58

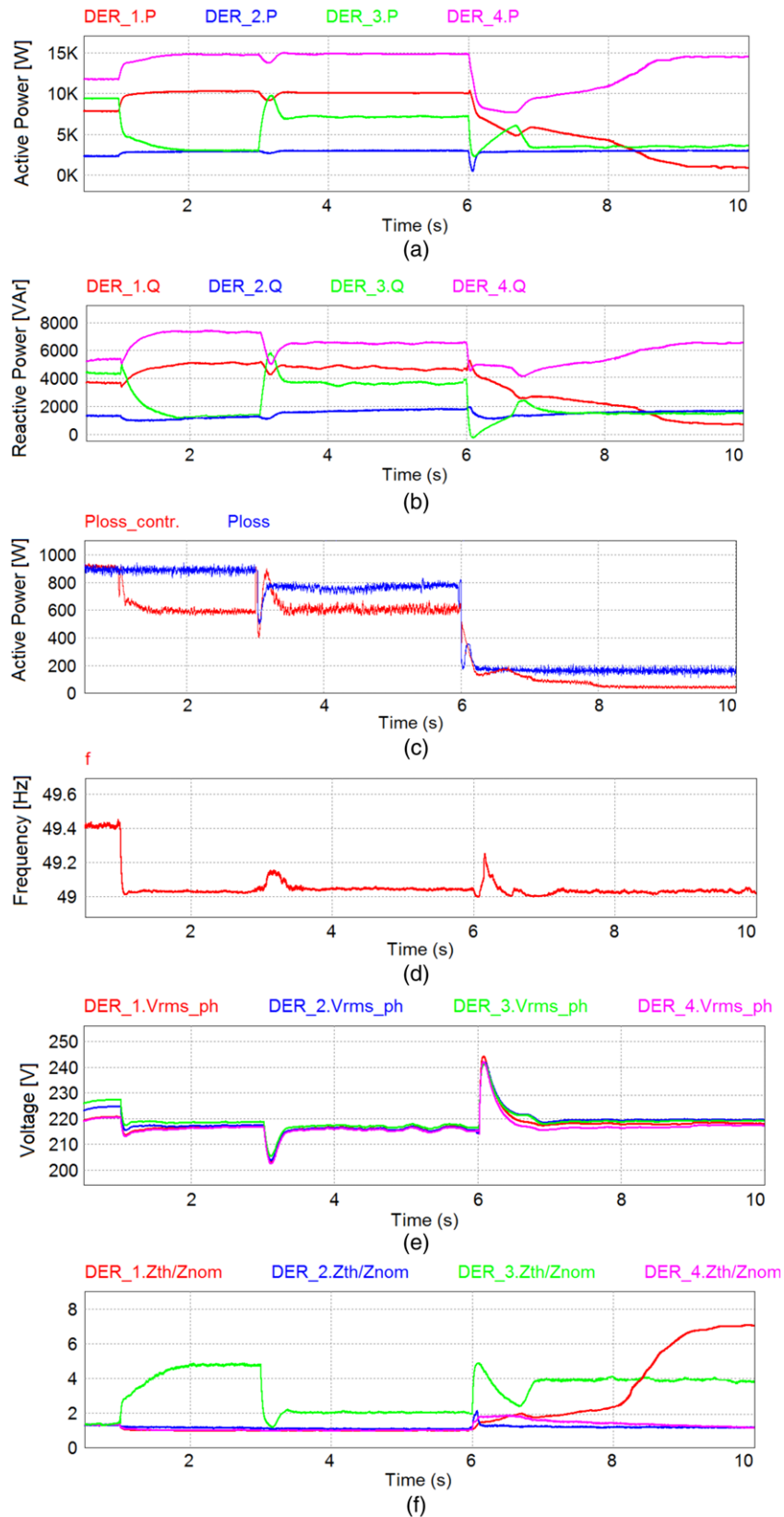


**Fig. 8.** Microgrid simulation results for a looped microgrid: (a) active power (W), (b) reactive power (VAr), (c) power losses (W), (d) frequency (Hz), (e) rms phase voltage (V), (f) microgrid impedance to nominal impedance ratio.

sharing to 599 W with the proposed control). It can be noticed that  $L_3$  is actually fed by DER<sub>3</sub>, since it is closer to this load. Thus, the  $Z_{th}/Z_{nom}$  ratio of DER<sub>3</sub> is significantly reduced (Fig. 8(f)), while the  $Z_{th}/Z_{nom}$  ratio of the other DERs remains almost unaffected.

#### 4.2.3. Case study 3: looped microgrid with disconnection of $L_1$

Finally, at  $t = 6$  s,  $L_1$  is disconnected by opening  $sw_4$ . As a result, the measured Thevenin impedances are automatically updated

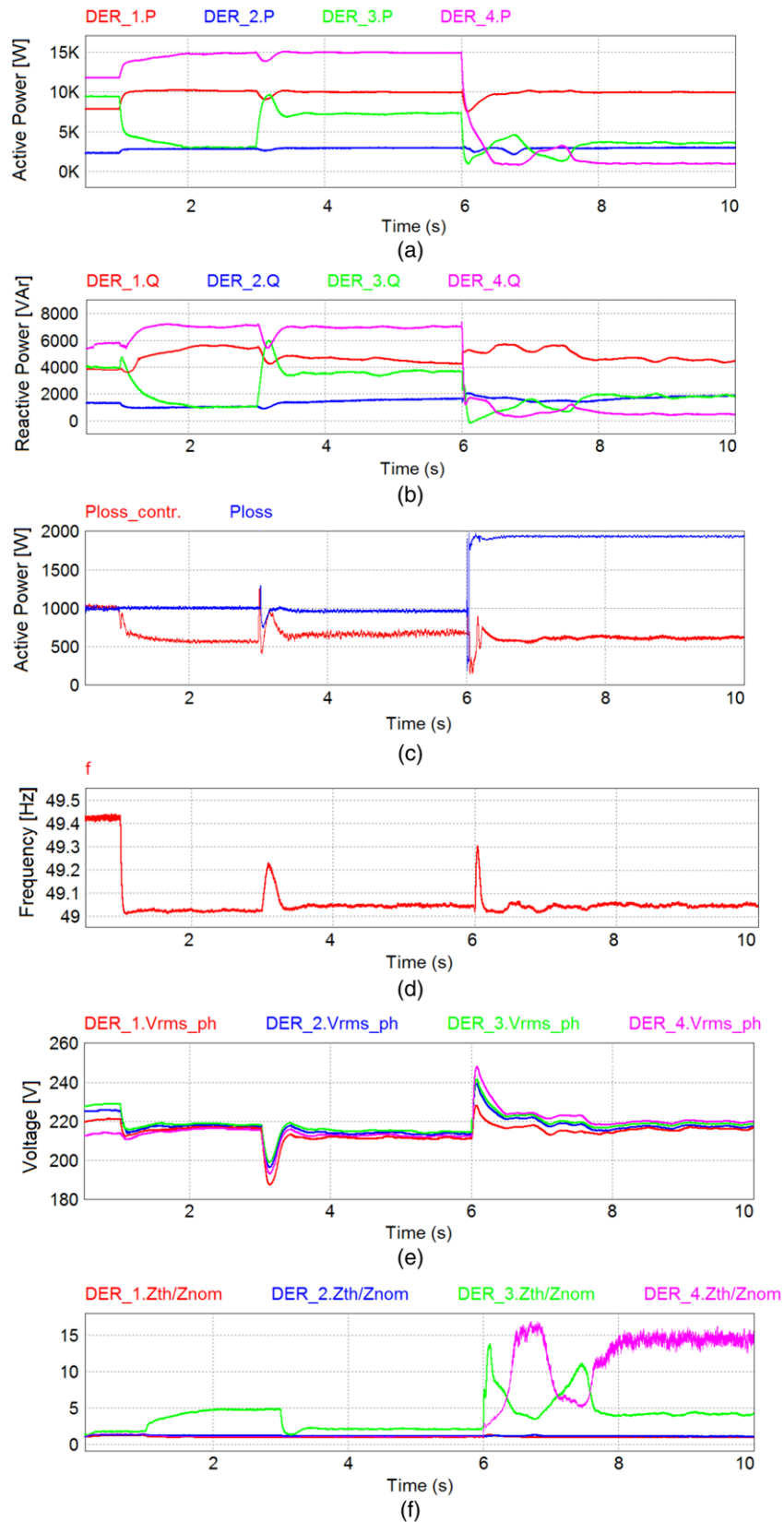


**Fig. 9.** Microgrid simulation results for a radial microgrid: (a) active power (W), (b) reactive power (VAr), (c) power losses (W), (d) frequency (Hz), (e) rms phase voltage (V), (f) microgrid impedance to nominal impedance ratio.

and thus the active and reactive power distribution changes, according to Fig. 8(a), (b). Since the load  $L_1$  absorbed a relatively large amount of power, the microgrid settles after a larger

transient, compared to the previous case study. The frequency and the voltages are not affected significantly, since their values were near to the minimal permitted. At the final operation point,

DER<sub>1</sub> contributes with less power since the impedance it senses increases significantly (Fig. 8(f)). On the contrary, DER<sub>2</sub> senses only a minor change in its impedance because L<sub>1</sub> were 1500 m apart. For this reason the power injected by DER<sub>2</sub> remains unaffected. The power losses are still reduced with respect to the corresponding of the accurate power sharing mode (from 164 to 57 W, i.e. 34.75% reduction).

It is evident from the results in the looped topology that the DERs adjust continuously their droop coefficients in order to follow the changes in the location and size of the loads. In this way, the loads are covered by the DERs which are relatively closer to them resulting in reduced line losses with respect to the accurate power sharing methodology.

#### 4.3. Microgrid with 4 DERs in radial topology

The final simulation test is conducted in a radial microgrid. In order to form the radial topology, switches sw<sub>2</sub> and sw<sub>3</sub> open, isolating Line<sub>6</sub> in Fig. 7.

##### 4.3.1. Case study 4: radial microgrid with L<sub>1</sub> and L<sub>2</sub> connected

Initially, L<sub>3</sub> is also disconnected (sw<sub>1</sub> is open) and the microgrid operates with the conventional droop control. Compared to the previous simulation results, the microgrid topology changes from looped to radial, which corresponds to new settings of the virtual impedance in order to ensure an accurate power sharing operation. The respective values are presented in Table 3. At  $t = 1$  s, the droop coefficients are changed adaptively in proportion to the sensed  $Z_{th}/Z_{nom}$  ratio (Fig. 9(f)). The active and reactive power sharing is also adjusted (Fig. 9(a), (b)), resulting in change of the frequency and voltages of the DERs (Fig. 9(d), (e)). It can be noticed that L<sub>1</sub> is mainly fed by DER<sub>1</sub> and DER<sub>2</sub>, which are 300 m and 1500 m apart from it respectively. For this reason, these two DERs reach their maximum available power. Since at least one DER must operate at its maximum power, it is reasonable that the frequency will settle to the lower permissible value ( $\sim 49$  Hz) as shown in Fig. 9(d). DER<sub>4</sub> also reaches its maximum power covering the largest part of L<sub>2</sub>, while the remaining power is fulfilled by DER<sub>3</sub>. The voltages take the same value for each DER, while the power losses are reduced from 981.4 to 591.4 W (39.73% loss reduction), as presented in Fig. 9(c). Thus, the proposed control strategy can reduce the power losses irrespective of the microgrid topology.

##### 4.3.2. Case study 5: radial microgrid with connection of L<sub>3</sub>

At  $t = 3$  s, L<sub>3</sub> is connected to the microgrid. The frequency and the node voltages are slightly affected (Fig. 9(d), (e)). At the new operation point, the power losses are reduced from 971 W with accurate power sharing to 678 W with the proposed control. Similar to the analysis of the looped topology, L<sub>3</sub> is mainly fed by DER<sub>3</sub>. The  $Z_{th}/Z_{nom}$  ratio of DER<sub>3</sub> is significantly reduced (Fig. 9(f)), while the  $Z_{th}/Z_{nom}$  ratio of the other DERs remains almost the same.

##### 4.3.3. Case study 6: radial microgrid with disconnection of L<sub>2</sub>

At  $t = 6$  s, L<sub>2</sub> is disconnected (sw<sub>5</sub> opens). The measured Thevenin impedances are updated again (Fig. 9(f)) and the active and reactive power distribution changes, according to Fig. 9(a), (b). Since now DER<sub>4</sub> is farther from the loads, it contributes with less power. DER<sub>3</sub> should cover only L<sub>3</sub>, thus its power decreases too. The frequency and the node voltages appear in Fig. 9(d), (e), which results in a new operation point. At this operation point, the power losses are 628 W, while implementing the accurate power sharing methodology the losses would be 1935 W (Fig. 9(c)), because all the DERs would supply L<sub>1</sub> and L<sub>3</sub> with active and reactive power in proportion to their nominal power, independently of their distance from the loads.

## 5. Conclusions

This paper proposes a new power sharing methodology that aims to reduce the line losses in an islanded converter-dominated microgrid without using communication. The control strategy utilizes the droop control method with adaptive droop coefficients. The droop coefficients are adjusted by the measured microgrid impedance, as it is sensed by each DER. Compared to the accurate power sharing method, the DERs closer to the loads are forced to supply relatively larger power than the DERs far from the loads. Thus, the currents within the microgrid flow through lower impedance routes, resulting in reduction of the line losses. The proposed method is equally effective for both radial and looped topologies, without considering any further regulation on the control strategy, while the number and the location of the DERs and the loads can be arbitrary. Additionally, since no communication infrastructure is necessary, the function of power loss reduction is actually implemented in the primary control level. In the literature, on the contrary, the economic operation of the microgrid is performed in the secondary control level, which requires a communication among the DERs and a central controller. Another advantage of the proposed adaptive droop control strategy is the inherent decoupling of the active and reactive power. For this reason, the virtual impedance regulation is no longer needed. The proposed control strategy is verified by comparison with the accurate power sharing method, which is commonly used in islanded microgrids implementing fully decentralized control.

## References

- [1] M. Soshinskaya, H.J. Wina Crijns-Graus, J.M. Guerrero, J.C. Vasquez, Microgrids: Experiences, barriers and success factors, *Renewable Sustainable Energy Rev.* 40 (2014) 659–672.
- [2] J.M. Guerrero, L. Garcia De Vicuna, J. Matas, M. Castilla, J. Miret, A wireless controller to enhance dynamic performance of parallel inverters in distributed generation systems, *IEEE Trans. Power Electron.* 19 (5) (2004) 1205–1213.
- [3] I.J. Balaguer, Lei Qin, Yang Shuitao, U. Supatti, Peng Fang Zheng, Control for grid-connected and intentional islanding operations of distributed power generation, *IEEE Trans. Ind. Electron.* 58 (1) (2011) 147–157.
- [4] Seon-Ju Ahn, Jin-woo Park, Il-Yop Chung, Seung-Il Moon, Sang-Hee Kang, Soon-Ryul Nam, Power-sharing method of multiple distributed generators considering control modes and configurations of a microgrid, *IEEE Trans. Power Deliv.* 25 (3) (2010) 2007–2016.
- [5] J.M. Guerrero, M. Chandorkar, T. Lee, P.C. Loh, Advanced control architectures for intelligent microgrids—part I: Decentralized and hierarchical control, *IEEE Ind. Electron.* 60 (4) (2013) 1254–1262.
- [6] J.M. Guerrero, J.C. Vasquez, J. Matas, L.G. de Vicuña, M. Castilla, Hierarchical control of droop-controlled AC and DC microgrids—a general approach toward standardization, *IEEE Ind. Electron.* 58 (1) (2011) 158–172.
- [7] D.E. Olivares, A. Mehrizi-Sani, A.H. Etemadi, C.A. Canizares, R. Iravani, M. Kazerani, A.H. Hajimiragha, O. Gomis-Bellmunt, M. Saadedifard, R. Palma-Behnke, G.A. Jimenez-Estevéz, N.D. Hatziaargyriou, Trends in microgrid control, *IEEE Trans. Smart Grid* 5 (4) (2014) 1905–1919.
- [8] J.M. Guerrero, L. Garcia De Vicuna, J. Matas, M. Castilla, J. Miret, Output impedance design of parallel-connected UPS inverters with wireless load-sharing control, *IEEE Trans. Ind. Electron.* 52 (4) (2005) 1126–1135.
- [9] J.M. Guerrero, J. Matas, L.G. de Vicuna, M. Castilla, J. Miret, Decentralized control for parallel operation of distributed generation inverters using resistive output impedance, *IEEE Trans. Ind. Electron.* 54 (2) (2007) 994–1004.
- [10] Wei Yao, Min Chen, J. Matas, J.M. Guerrero, Zhao-ming Qian, Design and analysis of the droop control method for parallel inverters considering the impact of the complex impedance on the power sharing, *IEEE Ind. Electron.* 58 (2) (2011) 576–588.
- [11] He Jinwei, Li Yun Wei, J.M. Guerrero, F. Blaabjerg, J.C. Vasquez, An islanding microgrid power sharing approach using enhanced virtual impedance control scheme, *IEEE Power Electron.* 28 (11) (2013) 5272–5282.
- [12] H. Mahmood, D. Michaelson, Jiang Jin, Accurate reactive power sharing in an islanded microgrid using adaptive virtual impedances, *IEEE Power Electron.* 30 (3) (2015) 1605–1617.
- [13] T.L. Vandoorn, J.D.M. De Koening, B. Meersman, J.M. Guerrero, L. Vandevelde, Automatic power-sharing modification of P/V droop controllers in low-voltage resistive microgrids, *IEEE Trans. Power Deliv.* 27 (4) (2012) 2318–2325.
- [14] A.R. Di Fazio, G. Fusco, M. Russo, Smart DER control for minimizing power losses in distribution feeders, *Electr. Power Syst. Res.* 109 (2014) 71–79.
- [15] M. Hamzeh, H. Mokhtari, H. Karimi, A decentralized self-adjusting control strategy for reactive power management in an islanded multi-bus MV microgrid, *Canad. J. Electr. Comput. Eng.* 36 (1) (2013) 18–25.

- [16] K. Turitsyn, P. Sulc, S. Backhaus, M. Chertkov, Distributed control of reactive power flow in a radial distribution circuit with high photovoltaic penetration, in: *IEEE Power and Energy Society General Meeting*, 2010, pp. 1–6.
- [17] V. Calderaro, G. Conio, V. Galdi, G. Massa, A. Piccolo, Optimal decentralized voltage control for distribution systems with inverter-based distributed generators, *IEEE Trans. Power Syst.* 29 (1) (2014) 230–241.
- [18] Changsun Ahn, Hwei Peng, Decentralized voltage control to minimize distribution power loss of microgrids, *IEEE Trans. Smart Grid* 4 (3) (2013) 1297–1304.
- [19] D.E. Olivares, C.A. Cañizares, M. Kazerani, A centralized energy management system for isolated microgrids, *IEEE Trans. Smart Grid* 5 (4) (2014) 1864–1875.
- [20] P. Arboleya, C. Gonzalez-Moran, M. Coto, A hybrid central-distributed control applied to microgrids with droop characteristic based generators, in: *Proceedings of the 15th International Power Electronics and Motion Control Conference, EPE/PEMC*, 2012.
- [21] E.R. Sanseverino, N.N. Quang, M.L. Di Silvestre, J.M. Guerrero, C. Li, Optimal power flow in three-phase islanded microgrids with inverter interfaced units, *Electr. Power Syst. Res.* 123 (2015) 48–56.
- [22] C.A. Hernandez-Aramburo, T.C. Green, N. Mugniot, Fuel consumption minimization of a microgrid, *IEEE Trans. Ind. Appl.* 41 (3) (2005) 673–681.
- [23] E. Barklund, N. Pogaku, M. Prodanovic, C. Hernandez-Aramburo, T.C. Green, Energy management in autonomous microgrid using stability-constrained droop control of inverters, *IEEE Trans. Power Electron.* 23 (5) (2008) 2346–2352.
- [24] P.H. Divshali, S.H. Hosseinian, M. Abedi, A novel multi-stage fuel cost minimization in a VSC-based microgrid considering stability, frequency, and voltage constraints, *IEEE Trans. Power Syst.* 28 (2) (2013) 931–939.
- [25] S. Conti, R. Nicolosi, S.A. Rizzo, H.H. Zeineldin, Optimal dispatching of distributed generators and storage systems for MV islanded microgrids, *IEEE Trans. Power Deliv.* 27 (3) (2012) 1243–1251.
- [26] A. Basu, A. Bhattacharya, S. Chowdhury, S.P. Chowdhury, Planned scheduling for economic power sharing in a CHP-based microgrid, *IEEE Trans. Power Syst.* 27 (1) (2012) 30–38.
- [27] A. Samadi, E. Shayesteh, R. Eriksson, B. Rawan, L. Söder, Multi-objective coordinated droop-based voltage regulation in distribution grids with PV systems, *Renew. Energy* 71 (2014) 315–323.
- [28] D. Fei, K.A. Loparo, Hierarchical decentralized network reconfiguration for smart distribution systems—part I: Problem formulation and algorithm development, *IEEE Trans. Power Syst.* 30 (2) (2015) 734–743.
- [29] W.T. Elsayed, E.F. El-Saadany, A fully decentralized approach for solving the economic dispatch problem, *IEEE Trans. Power Syst.* 30 (4) (2015) 2179–2189.
- [30] J.S. Heo, K.Y. Lee, A multiagent-system-based intelligent reference governor for multiobjective optimal power plant operation, *IEEE Trans. Energy Convers.* 23 (4) (2008) 1082–1092.
- [31] S. Bolognani, R. Carli, G. Cavraro, S. Zampieri, Distributed reactive power feedback control for voltage regulation and loss minimization, *IEEE Trans. Automat. Control* 60 (4) (2015) 966–981.
- [32] S. Kalambe, G. Agnihotri, Loss minimization techniques used in distribution network: bibliographical survey, *Renewable Sustainable Energy Rev.* 29 (2014) 184–200.
- [33] A.A. Bazmi, G. Zahedi, Sustainable energy systems: Role of optimization modeling techniques in power generation and supply—a review, *Renewable Sustainable Energy Rev.* 15 (8) (2011) 3480–3500.
- [34] M. Ciobotaru, V.G. Agelidis, R. Teodorescu, F. Blaabjerg, Accurate and less-disturbing active antiislanding method based on PLL for grid-connected converters, *IEEE Power Electron.* 25 (6) (2010) 1576–1584.
- [35] **Voltage characteristics of electricity supplied by public distribution system, standard EN 50160:2004.**
- [36] K.O. Oureilidis, C.S. Demoulias, An enhanced role for an energy storage system in a microgrid with converter-interfaced sources, *J. Eng.* (2014).